High-Q antennas: Simulator limitations

Barrio, Samantha Caporal Del; Pedersen, Gert Frølund

Published in:
Antennas and Propagation (EuCAP), 2013 7th European Conference on

Publication date:
2013

Document Version
Early version, also known as pre-print

High-Q Antennas: Simulator limitations

Samantha Caporal Del Barrio*, Gert F. Pedersen*
*Section of Antennas, Propagation and Radio Networking (APNet), Department of Electronic Systems,
Faculty of Engineering and Science, Aalborg University, DK-9220, Aalborg, Denmark
{scdb, gfp}@es.aau.dk

***Abstract*—Increasing the mesh steps - i.e. the accuracy of the model - of a structure leads to converging results towards reality. With high-field structures, discretization of the domain in a transient simulation becomes of important matter. It is shown in this work that for these structures convergence of the results does not seem to happen with surface current and efficiency calculations.**

***Index Terms*—Numerical simulation; Mobile antennas; Antenna measurement.**

I. Introduction

The demand from mobile phone users for more connectivity led the development of the 4^{th} Generation (4G) of mobile communication systems. 4G uses the new Long Term Evolution (LTE) technology to provide very high data rates; up to 1 Gbps with LTE-Advanced [1]. In order to meet high-speed data transfers LTE architecture includes multiple antennas at the base station (BS) and in the User Equipment (UE). It also includes a larger frequency spectrum for mobile communications from 700 MHz to 2.6 GHz, with at least 20 different bands [1].

A major challenge that LTE raises for the handsets antenna engineers is designing antennas that cover a very large bandwidth and that fit in a very small volume. On the one hand the available space for one antenna has suffered a great reduction. This phenomenon is due to the integration of more components in the mobile phone thus enforcing size reduction. Additionally, to comply with LTE architectures several antennas need to fit into this already reduced space allocated for the antennas. On the other hand antenna bandwidth is directly related to the antenna size as demonstrated in [2]. Therefore for a given volume the achievable bandwidth has a limit [3] and in order to cover the 4G spectrum traditional antenna designs will have a very large volume.

Frequency-Reconfigurable Antennas (FRA) are active elements that use a switch or a tunable component in order to modify the resonance frequency of the resulting antenna. They are very good candidates for 4G, as a unique and small element can be used to cover several bands. However the difficulty with FRA is their rather high Quality factor (Q). Indeed the Q of an antenna increases as its size decreases [3], moreover the Q of a FRA increases as the antenna element is tuned away from the Ground Plane (GP) resonance [4]. Therefore small FRA are expected to have a very high Q, and commonly high-Q structures exhibit high losses [5]. This study focuses on high-Q FRA at frequencies between 700 MHz and 1GHz.

In this study simulated and measured performances of high-Q antennas are compared. Section II presents the simulation parameters that are used for modeling the structure and Section III analyzes the differences between simulation and measurement. Section IV proposes a modeling of the loss mechanism of high-Q antennas. Finally Section V draws the conclusions.

II. Simulation parameters

A. Antenna Q

In the presented work Q refers to the Perfectly Matched Q at a given frequency ω_0. In [3] it is shown that $Q(\omega_0)$ is related to the matched Fractional Bandwidth (FBW) at a given voltage standing wave ratio (s). The following formula is used throughout the paper for evaluating Q:

$$Q(\omega_0) \approx \frac{2\sqrt{\beta}}{FBW_s(\omega_0)}, \sqrt{\beta} = \frac{s-1}{2\sqrt{s}}. \quad (1)$$

B. Antenna design

A Planar-Inverted-F Antenna (PIFA) resonating at 960 MHz is designed for a Personal Digital Assistant (PDA) form factor with dimensions 119 x 59 mm^2. The height (h) of the PIFA over the Ground Plane (GP) determines the Q of the structure. Here h is fixed to 4 mm and leads to $Q = 14$ at 960 MHz. Details on the geometry of the antenna element are shown in Fig. 1. A tunable capacitor is placed between the PIFA and the GP in order to modify the reactance of the resulting antenna and to shift its resonance frequency. The tunable capacitor is placed at 10 mm from the feed point. As the value of the capacitor increases the resonance frequency of the tunable antenna decreases and its Q increases.

The study is made for three distinct frequencies arbitrarily chosen throughout the LTE low-band: 960 MHz, 745 MHz and 700 MHz. The frequency 900 MHz belongs to the common GSM standard (or band 8 for LTE), the frequencies 745 MHz and 700 MHz belong to the bands 12, 13 and 17 where Verizon and AT&T deploy 4G LTE equipments in the U.S. The lowest frequency bands are the most challenging bands from an antenna design point of view as the antenna is electrically small and the whole Ground Plane (GP) is also part of the radiation mechanism.

C. Simulation accuracy

This work investigates the impact on the simulation results of the meshing of a high-Q structure in the transient solver of CST [6]. The antenna and the GP are made in copper with a

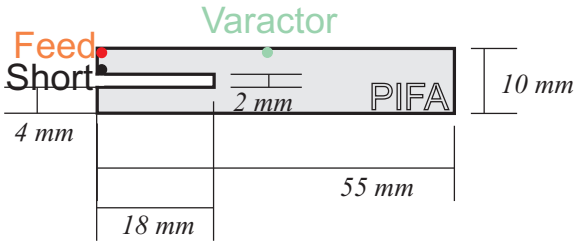

Fig. 1. Antenna design.

conductivity $\sigma = 5.80 * 10^7$ S/m, which has a wavelength of $\lambda_{900} = 1.57 * 10^{-5}$ m at 900 MHz. Results with 6 meshing levels are compared. The meshing is controlled with the "refinement factor" parameter and all other parameters are fixed for comparison purposes. The fixed parameters are listed in Table I. Some of them where set to the default value when acceptable. These parameters are kept identical throughout the investigation in order to isolate the impact of the meshing of the structure only. The meshing accuracy is plotted in Fig. 2 from a top view in order to show the connection of the tuning capacitor between the PIFA and the GP, as this is where the high fields concentrate throughout tuning. The accuracy levels of the meshing are denoted with the number of cells contained in 1 mm^2 of the tuning component area (port 2). The computational time of the simulation increases dramatically with the mesh accuracy, it is shown in Table II in order to get a feeling of the cost of increasing the accuracy of the simulations.

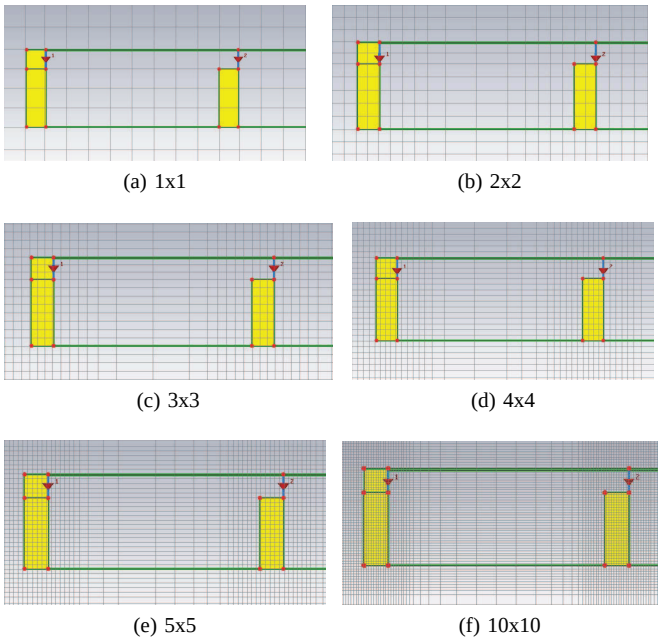

(a) 1x1 (b) 2x2

(c) 3x3 (d) 4x4

(e) 5x5 (f) 10x10

Fig. 2. Simulation accuracy (port 1 is the source, port 2 is the capacitor).

TABLE I
FIXED PARAMETERS THROUGHOUT SIMULATIONS

Maximum lines per wavelength	30
Minimum lines per wavelength	20
Eq mesh ratio	1.19
Max cell ratio	10
Energy criteria	-80 dB

TABLE II
SIMULATION TIME

Meshing	Simulation time
1x1	178 s (= 0 h, 2 m, 58 s)
2x2	734 s (= 0 h, 12 m, 14 s)
3x3	2300 s (= 0 h, 38 m, 20 s)
4x4	4981 s (= 1 h, 23 m, 1 s)
5x5	10949 s (= 3 h, 2 m, 29 s)
10x10	88438 s (= 24 h, 33 m, 58 s)

D. Tuning

The antenna aims at being fine-tuned from 960 MHz to 700 MHz. Continuous tuning can be done with a tunable Micro-Electro Mechanical System (MEMS) capacitor; for example [7] can deliver tuning steps of 1/8 pF - from 1/8 pF to 8 pF. In order to simplify the measurements low-loss Murata GJM15 fixed capacitors will be used [8]. The Equivalent Series Resistances (ESR) of the capacitors are input in the simulations. For comparison purposes they are set to be constant throughout the accuracy steps, even though the capacitance may slightly change. The schematic of the tuning is shown in Fig. 3. On the right side of the antenna block, C1 represents the capacitance of the tuning component and R1 represents the ESR of C1. On the left side of the antenna block, L1 and C2 represent a lossless matching network. The matching is done in order to have comparable accepted power in the antenna and the tuning capacitor throughout the simulations, to be able to compare the efficiency results. All computations are normalized to 1 W input power.

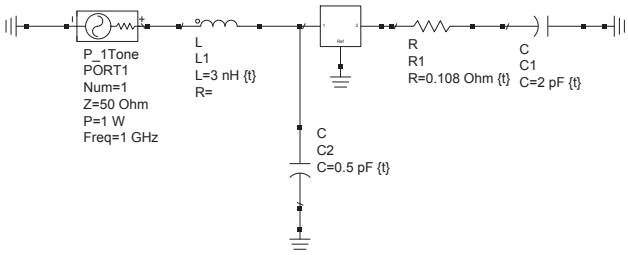

Fig. 3. Tuning schematic.

III. RESULTS AND INTERPRETATION

The simulation analysis is made for the three frequencies 900 MHz, 745 MHz and 700 MHz. A mock-up of the antenna design is built and the measured results are compared to the simulation results.

TABLE III
BW AND Q

	Meshing	C [pF]	ESR [Ω]	BW [MHz]	Q
900 MHz	1x1	1.125	0.11	49.2	18.3
	2x2	1.125	0.11	50.1	17.9
	3x3	1.125	0.11	49.7	18.1
	4x4	1.125	0.11	48.1	18.7
	5x5	1.125	0.11	48.0	18.7
	10x10	1.125	0.11	48.3	18.6
745 MHz	1x1	3.625	0.115	11.3	65.9
	2x2	3.375	0.115	11.7	63.7
	3x3	3.375	0.115	11.4	65.3
	4x4	3.25	0.115	11.7	63.7
	5x5	3.25	0.115	11.5	64.8
	10x10	3.25	0.115	11.3	65.9
700 MHz	1x1	4.375	0.108	7.5	93.3
	2x2	4.125	0.108	7.7	90.9
	3x3	4	0.108	7.6	92.1
	4x4	4	0.108	7.5	93.3
	5x5	3.875	0.108	7.6	92.1
	10x10	3.875	0.108	7.5	93.3

A. Bandwidth and Q

The results on the bandwidth for a fixed Voltage Standing Wave Ratio (VSWR) of -7 dB with a perfect match (BW) and the results on the Q values - depending on the meshing accuracy - are summarized in Table III. The antenna Q is 14 at 960 MHz. Therefore when the antenna is tuned from 960 MHz to 900 MHz the structure is considered low-Q hereafter. When the antenna is tuned to 745 MHz and 700 MHz the Q value rises significantly and the antenna is considered high-Q hereafter. In the first part of the Table III the antenna is tuned to 900 MHz; increasing the accuracy of the mesh leads to higher accuracy in the results as expected. The value of the capacitance needed to tune the resonance frequency is unchanged throughout the simulations with denser mesh. The ESR is voluntarily fixed to 0.11 Ω as specified in [8] for that particular capacitance. The BW constantly decreases from 50 MHz to 48 MHz; correspondingly the Q value increases constantly. In the second and third part of the Table III, the antenna has a higher Q and the tendency with denser mesh is not clear. The capacitance needed in order to tune the antenna is decreased as the mesh density increases and results for BW and Q fluctuate, instead of converging to an accurate value. These results indicate that the results obtained for high-Q structures are not precise with the transient solver.

B. Surface currents

This section investigates the evolution of the surface currents throughout simulations with increasing mesh accuracy. Surface currents plots are shown in Fig. 4. Two mesh types are shown as example but the conclusions are drawn out of all the simulations. Both low-Q and high-Q structures exhibit surface currents that are not constant with increasing mesh accuracy. At 900 MHz the highest surface current is located

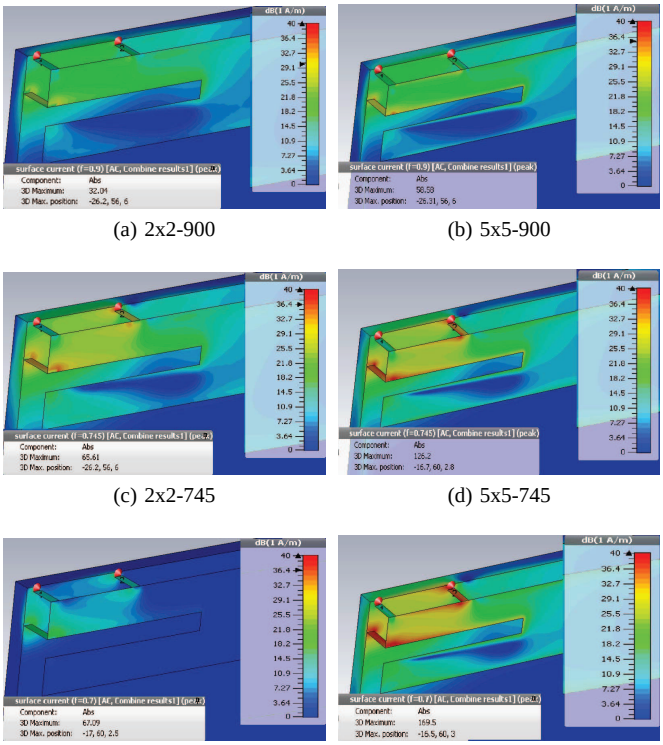

(a) 2x2-900 (b) 5x5-900

(c) 2x2-745 (d) 5x5-745

(e) 2x2-700 (f) 5x5-700

Fig. 4. Surface currents.

at the short and the peak current evolves from 32 dBA/m with the 2×2 mesh (see Fig. 4a) to 58 dBA/m with the 5×5 mesh (see Fig. 4b). At 700 MHz the highest surface current evolves from being located at the short with a value of 67 dBA/m with the 2×2 mesh (see Fig. 4e) to being located at the capacitor with a value of 169 dBA/m with the 5×5 mesh (see Fig. 4f). Differences between peak surface currents are large and highly depend on the meshing of the structure. They do not seem to converge to a finite value and rather dramatically increase. However surface currents do not fluctuate throughout all the simulations with increasing mesh accuracy.

C. Current magnitude delivered to the capacitor

The magnitudes of the current delivered to the capacitor throughout tuning are computed. On their computation relies the accuracy of the loss calculation as the ESR of the capacitor is a considerable source of loss; which is proportional to the square of the currents. The currents are computed with ADS software [9] and the results are summarized in Table IV. The values of the currents delivered to the capacitor do not seem to converge towards a certain value and rather seem to constantly increase, as the surface currents did. The consequence of this is represented in Table V where the loss due to the ESR does not to converge either.

D. Efficiencies

The Table V shows the efficiency calculation for the high-Q antenna with increasing mesh accuracy. E_T is the total

TABLE IV
CURRENTS

	Meshing	I_{cap} [A]	Normalized I_{cap} [A/pF]
900 MHz	1x1	0.204	0.181
	2x2	0.208	0.185
	3x3	0.211	0.188
	4x4	0.214	0.190
	5x5	0.215	0.191
	10x10	0.19	0.19
745 MHz	1x1	1.093	0.302
	2x2	1.027	0.304
	3x3	1.054	0.312
	4x4	1.01	0.311
	5x5	1.026	0.316
	10x10	1.039	0.320
700 MHz	1x1	1.480	0.338
	2x2	1.422	0.345
	3x3	1.389	0.347
	4x4	1.410	0.353
	5x5	1.363	0.352
	10x10	1.374	0.355

TABLE V
EFFICIENCIES IN DB

	Mesh	E_T	$E_{r,id}$	$E_{L,ESR}$	$E_{T,est}$
900 MHz	1x1	-0.08	-0.07	-0.01	-0.08
	2x2	-0.09	-0.08	-0.01	-0.09
	3x3	-0.10	-0.09	-0.01	-0.10
	4x4	-0.10	-0.09	-0.01	-0.10
	5x5	-0.11	-0.10	-0.01	-0.11
	10x10	-0.12	-0.11	-0.01	-0.12
745 MHz	1x1	-0.61	-0.30	-0.31	-0.61
	2x2	-0.62	-0.35	-0.27	-0.62
	3x3	-0.66	-0.38	-0.29	-0.67
	4x4	-0.66	-0.40	-0.26	-0.66
	5x5	-0.69	-0.42	-0.27	-0.69
	10x10	-0.73	-0.45	-0.28	-0.73
700 MHz	1x1	-1.08	-0.53	-0.55	-1.08
	2x2	-1.12	-0.60	-0.50	-1.10
	3x3	-1.14	-0.65	-0.48	-1.13
	4x4	-1.18	-0.68	-0.49	-1.17
	5x5	-1.18	-0.71	-0.46	-1.17
	10x10	-1.24	-0.76	-0.47	-1.23

efficiency given by CST including the losses from the copper conductivity and from the ESR of the capacitor. These values are compared to the estimated total efficiency $E_{T,est}$, which is the sum of the radiation efficiency for an ideal capacitor (without ESR) $E_{r,id}$ given by CST, and the loss in the ESR $E_{L,ESR}$ computed from the currents in ADS. This means that $E_{T,est} = E_{r,id} + E_{L,ESR}$. It is worth noting that the frequency responses are perfectly match with lossless components in order to fairly compare simulations, therefore there is no mismatch loss to take into account. Firstly efficiencies computed with CST - E_T - and efficiencies estimated from the conductive and component loss separately - $E_{T,est}$ - are in very good agreement. Secondly the differences relative to the meshing are larger in the estimation of the conductive loss $E_{r,id}$ than in the estimation of the ESR loss $E_{L,ESR}$. Therefore the impact of the miscalculation of the surface currents can be neglected. The driving factor of the difference in total efficiency (Δ_{ET}) is the estimation of the thermal loss due to the lossy metal. Moreover this misestimation becomes worse with increasing Q. As a result Δ_{ET} is about 10 times more for the higher Q structure at 700 MHz than the lower Q structure at 900 MHz.

E. Measurements

A mock-up of the simulated antenna is built and shown in Fig. 5. It is tuned and measured; the frequency response is compared to the simulations in Fig. 6. At 900 MHz the simulated reflection coefficients are located in the upper part of the smith chart and they are rather close to each other. Due to building imprecision the mock-up response is slightly more inductive. At 700 MHz the simulated responses differ significantly from each other. Under-meshing or over-meshing of the antenna structure leads to inaccurate results compared to the mock-up. Then, the mock-up is measured in anechoic chamber. Efficiencies are computed with 3D radiation pattern integration technique and the results are shown in Table VI. The ESR of the capacitor in the simulation is equal to the one in the mock-up for comparison purposes. Mismatch loss and cable loss are subtracted from the total measured efficiency of the mock-up. It is observed that the measured efficiencies decrease dramatically with frequency. Moreover measured values are significantly lower than simulated values and degrade more rapidly. These observations confirm that properties of high-Q antennas are not accurately taken into account at the simulation level.

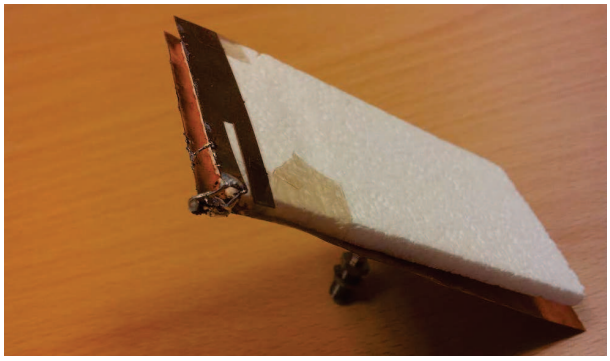

Fig. 5. Mock-up.

TABLE VI
MEASUREMENTS.

	C_{tun} [pF]	ESR [Ω]	Q_{PM}	E_T [dB]
960 MHz	0	0	8.9	-0.5
900 MHz	1.1	0.107	12.6	-1.5
745 MHz	3.3	0.114	42.8	-3
700 MHz	4	0.108	63.6	-4

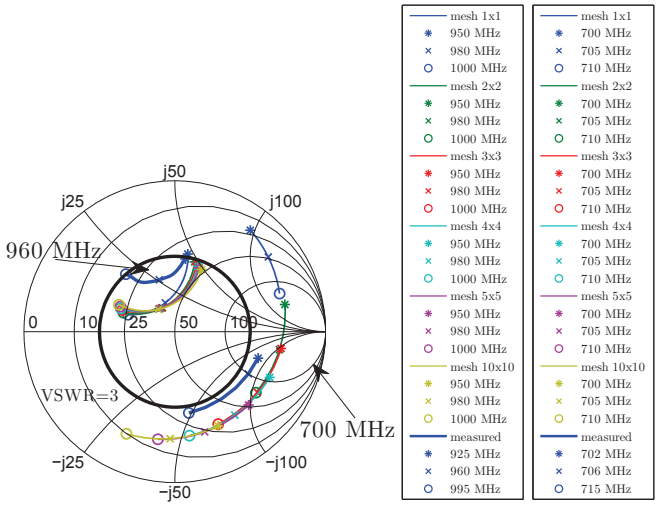

Fig. 6. Simulated and measured reflection coefficient.

IV. A POSSIBLE SOURCE OF LOSS

The previous sections show that the simulated and measured efficiencies differ significantly. The simulations show optimistic results. This section investigates the possibility of losses coming from the soldering tin.

In the schematic used to calculate the efficiency, resistances are added at the places where soldering tin is used on the mock-up. At the short, at the source and at the capacitor, a resistance corresponding to the use of the tin is added. The new schematic can be seen in Fig. 7 where the tin resistance is circled in red. The resistance of the tin was arbitrarily chosen to be 0.3 Ω. The simulation with a 3×3 mesh is re-evaluated with the tin resistance. The simulation with 3×3 mesh is chosen as it is the closest response on the Smith chart in Fig. 6 to the measured response. New simulated efficiencies are summarized in Table VII. The efficiencies are closer to the measured values.

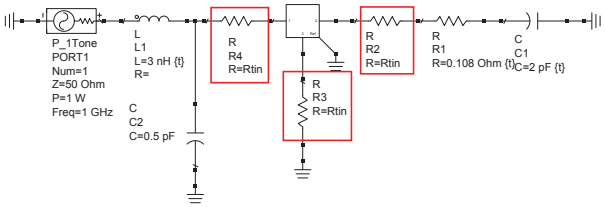

Fig. 7. Tuning schematic with tin loss.

TABLE VII
INFLUENCE OF THE TIN

Frequency [MHz]	Er [dB]
900	-0.5
745	-2.5
700	-4.0

V. CONCLUSION

This study presents simulated and measured performances of a high-Q FRA. Simulations are run with a transient solver and increasing mesh accuracy is tested. Comparisons with measurement results show that the loss mechanism of high-Q reconfigurable structures cannot be captured by simple simulations. Surface currents and conductive losses do not converge to a finite value when the accuracy of the simulations increases to a very fine mesh. As a result simulations predict lower losses than measurements show. On the one hand the difference may come from a misestimation of the loss due to the conductivity of the lossy metal with high fields. On the other hand a source of loss may have been neglected, as for example the effect of the soldering tin in presence of high fields. Having a correct loss estimation at the design step of a tunable structure is essential as they can be dramatically high. In order to improve the prediction of the efficiency of a high-Q FRA, other solvers can be tested or other source of losses as copper roughness can be modeled.

REFERENCES

[1] 3GPP Technical Report, “Feasibility study for Further Advancements for E-UTRA (LTE-Advanced) - Specification 36.912 - Release 11,” 2012.
[2] R. F. Harrington, “Effect of Antenna Size on Gain , Bandwidth , and Efficiency,” *Journal of Research of the National Bureau of Standards- D. Radio Propagation*, vol. 64D, no. 1, pp. 1–12, 1960.
[3] A. D. Yaghjian, S. R. Best, and S. Member, “Impedance , Bandwidth , and Q of Antennas,” *IEEE Transactions on Antennas and Propagation*, vol. 53, no. 4, pp. 1298–1324, 2005.
[4] P. Vainikainen, J. Ollikainen, O. Kivekäs, and I. Kelander, “Resonator-Based Analysis of the Combination of Mobile Handset Antenna and Chassis,” *IEEE Transactions on Antennas and Propagation*, vol. 50, no. 10, pp. 1433–1444, 2002.
[5] S. Caporal, D. Barrio, M. Pelosi, G. F. Pedersen, and A. Morris, “Challenges for Frequency-Reconfigurable Antennas in Small Terminals,” in *Vehicular Technology Conference*, 2012.
[6] Computer Simulation Technology, “CST MICROWAVE STUDIO.”
[7] WiSpry, “Tunable Digital Capacitor Arrays (TDCA).”
[8] Murata, “Chip Monolithic Ceramic Capacitors,” 2012.
[9] Agilent EEsof EDA, “Advanced Design System (ADS).”